

SUPPLEMENTAL DATA

Mechanical Forces

of Fission Yeast Growth

Nicolas Minc, Arezki Boudaoud, and Fred Chang

Theoretical Model

a- Viscoplastic Model for Cell Growth in Fission Yeast

We describe the fission yeast cell as a cylinder of radius R , and total length L . The intracellular turgor pressure P , is assumed to be homogeneous within the cell. The cell wall is also described as a homogeneous elastic material with Young's modulus E_{cw} and thickness h , yielding a surface modulus, $\sigma_{cw} = hE_{cw}$ (Figure 1A). Localized secretion and deposition of new cell wall allows for fission yeast cell growth to occur exclusively at the tips over a domain of length R [1]. The longitudinal (along the cell long axis) tension in the walls arising from the internal turgor pressure is:

$$T_p = \frac{PR}{2h}, \quad (\text{Eq. S1})$$

In the spirit of the models developed for plants [2-5], we assume that growth appears effectively as a viscoplastic process, where the free growth rate $v_0 = dL/dt$ is proportional to the strain T_p / E_{cw} in the wall in excess of a threshold plastic strain e_p . As growth occurs only in the cap of extension R , along the longitudinal axis:

$$v_0 = \frac{R}{\tau_V} \left(\frac{T_p}{E_{cw}} - e_p \right), \quad (\text{Eq. S2})$$

where τ_V is the viscoelastic time scale that encompasses the precise geometry of the cell tip, putative variations in the Young's modulus at the cell tip and the molecular timing involved in cell growth (polarity based distribution of cell wall remodeling factor).

The total turgor pressure, P , can thus be represented as the sum of a threshold pressure P_c needed for wall elongation and the effective turgor pressure $\Delta P = P - P_c$, that sets the growth rate. P_c can be estimated as the pressure needed to reach the plastic yield strain e_p : imposing $T_p / E_{cw} = e_p$ yields $P_c = \sigma_{cw} e_p / R \sim 0.1$ MPa when taking a plausible value $e_p = 1\%$, and the values measured of σ_{cw} in this study [6, 7]. Thus, replacing in Eq. (S2) leads to :

$$v_0 = \frac{1}{\tau_v} \frac{R^2}{2h} \frac{(P - P_c)}{E_{cw}} \quad (\text{Eq. S3})$$

b- Cell Buckling

Here, we consider the cell as an elastic rod where the elasticity arises from the cell wall layer. The energetic cost of buckling the cell is not affected by the turgor since it is compensated by the tension in the wall. The threshold force for buckling is thus given by:

$$F_B = \frac{\pi d E_{cw}}{L_T^2}, \quad (\text{Eq. S4})$$

with $I = \pi h R^3$, the second momentum of inertia of the cell wall layer, and L_T the distance between cell tips along the force axis [8]. Replacing with I and simplifying, Eq. (S4) leads to Eq. (2) presented in the main text.

c- Force Associated with Chamber Deformation

We compute the elastic force associated with the deformation d induced by the cell on the chamber by considering the PDMS chamber as an elastic solid being deformed by a cylinder, in that case [9]:

$$F = \frac{8}{3} E_{ch} R d \quad (\text{Eq. S5})$$

where the pre-factor 8/3 accounts for the geometrical configuration of a cylinder in contact with an elastic solid.

d- Cell Growth under Forces

Following Eq. S1, if the cell is growing under an external longitudinal force, F opposing growth (Figure 3B), the tension in the wall is reduced so that:

$$T = T_p - \frac{F}{2\pi R h}. \quad (\text{Eq. S6})$$

If we assume that τ_v is independent of the external force, then Eq. (S2) for the growth rate becomes:

$$v(F) = \frac{R}{\tau_v} \frac{T}{E}, \quad (\text{Eq. S6})$$

which, after straightforward simplifications yields:

$$v(F) = v_0 \left(1 - \frac{F}{\pi R^2 \Delta P} \right). \quad (\text{Eq. S7})$$

Equation S7 describes the change in velocity induced by the presence of an external force. We note that this change described by the ratio v/v_0 does not depend on τ_v and is thus independent of the local variations of the cell wall elastic modulus or the precise geometry of the cell.

e- Dynamic Evolution of Force and Growth Rate

In the configuration that we describe in the paper, the force, the velocity and the cell length change over time. The evolution of cell length can be obtained by replacing Eq. (S5) in Eq. (S7), so that:

$$\frac{1}{v_0} \frac{dL(t)}{dt} = 1 - \frac{8 E_{ch} R}{3 \Delta PS} (L(t) - D), \quad (\text{Eq. S8})$$

with D the microchamber diameter.

Eq. (S8) yields the evolution of cell length as a function of time:

$$L(t) = v_0 \tau_F (1 - e^{-t/\tau_F}) + D, \quad (\text{Eq. S10})$$

where time is measured from the contact with the obstacle. Here, we introduced τ_F , the characteristic time of growth stalling by the external force:

$$\tau_F = \frac{\Delta PS}{\frac{8}{3} E_{ch} R v_0} \quad (\text{Eq. S11})$$

The cell elongation follows an exponentially saturating behavior similar to the one we observe experimentally on Figure 3C. The force-velocity relation follows in turn a linear behavior described by Eq. (S7). This description allowed to match the behavior observed in all chambers (Figure 3C).

f- Dynamic of Cell Buckling

The last set of experiments consist of growing cells and studying whether they can buckle under the force of their own growth. The cell usually grows to the chamber border, slows down very rapidly and stops elongating for a given time, after which the cell buckles. By analyzing cells of different length, we saw that this delay before buckling, Δt , was inversely correlated with cell length. During the stalling phase, the cell is growing at a fixed length D , and is thus shortened from its reference length L by an amount $d=L-D$, so that the cell is submitted to a compressive strain d/L . This situation can be pictured as a coil that accumulates torsion without elongating. Using the elasticity of the cell wall, we obtain the force applied by the chamber on the cell:

$$F = 2\pi R \sigma_{cw} \frac{l}{L}, \quad (\text{Eq. S12})$$

Using the growth velocity $v=dd/dt$ and replacing in Eq. (S9) we obtain the external force evolution during the period of stalling ($0 < t < \Delta t$):

$$\frac{dF}{dt} + \frac{F}{\tau} = \frac{\Delta PS}{\tau}, \quad (\text{Eq. S13})$$

with a time-scale $\tau = \frac{L}{R} \tau_V$ (L is the cell length at buckling and we consider $l \ll D, L$).

The force exponentially relaxes to a maximum force equal to ΔPS :

$$F_B = \Delta PS \left(1 - e^{-\left(\frac{\Delta t}{\tau}\right)}\right), \quad (\text{Eq. S14})$$

Using values of v_0 and ΔP from the experiments and replacing in Eqs. (4,5), we expect τ in the range 5-30 min. The measured delays Δt range from 5-30 min and thus plotting F_B as a function of Δt should remain almost linear at all Δt which is consistent with observations (Figure 4C).

Supplemental References

1. Chang, F. (2001). Establishment of a cellular axis in fission yeast. *Trends Genet* 17, 273-278.
2. Lockhart, J.A. (1965). An Analysis of Irreversible Plant Cell Elongation. *Journal of Theoretical Biology* 8, 264-&.
3. Green, P.B., Erickson, R.O., and Buggy, J. (1971). Metabolic and Physical Control of Cell Elongation Rate - in-Vivo Studies in *Nitella*. *Plant Physiology* 47, 423-&.
4. Proseus, T.E., Ortega, J.K.E., and Boyer, J.S. (1999). Separating growth from elastic deformation during cell enlargement. *Plant Physiology* 119, 775-784.
5. Dumais, J., Shaw, S.L., Steele, C.R., Long, S.R., and Ray, P.M. (2006). An anisotropic-viscoplastic model of plant cell morphogenesis by tip growth. *International Journal of Developmental Biology* 50, 209-222.
6. Proseus, T.E., Ortega, J.K., and Boyer, J.S. (1999). Separating growth from elastic deformation during cell enlargement. *Plant Physiol* 119, 775-784.
7. Boudaoud, A. (2003). Growth of walled cells: from shells to vesicles. *Phys Rev Lett* 91, 018104.
8. Landau, L.D., and Lifshitz, E.M. (1959). *Theory of elasticity*, (MIR Moscow).
9. Johnson, K.L. (1987). *Contact Mechanics*, (Cambridge U. Press).

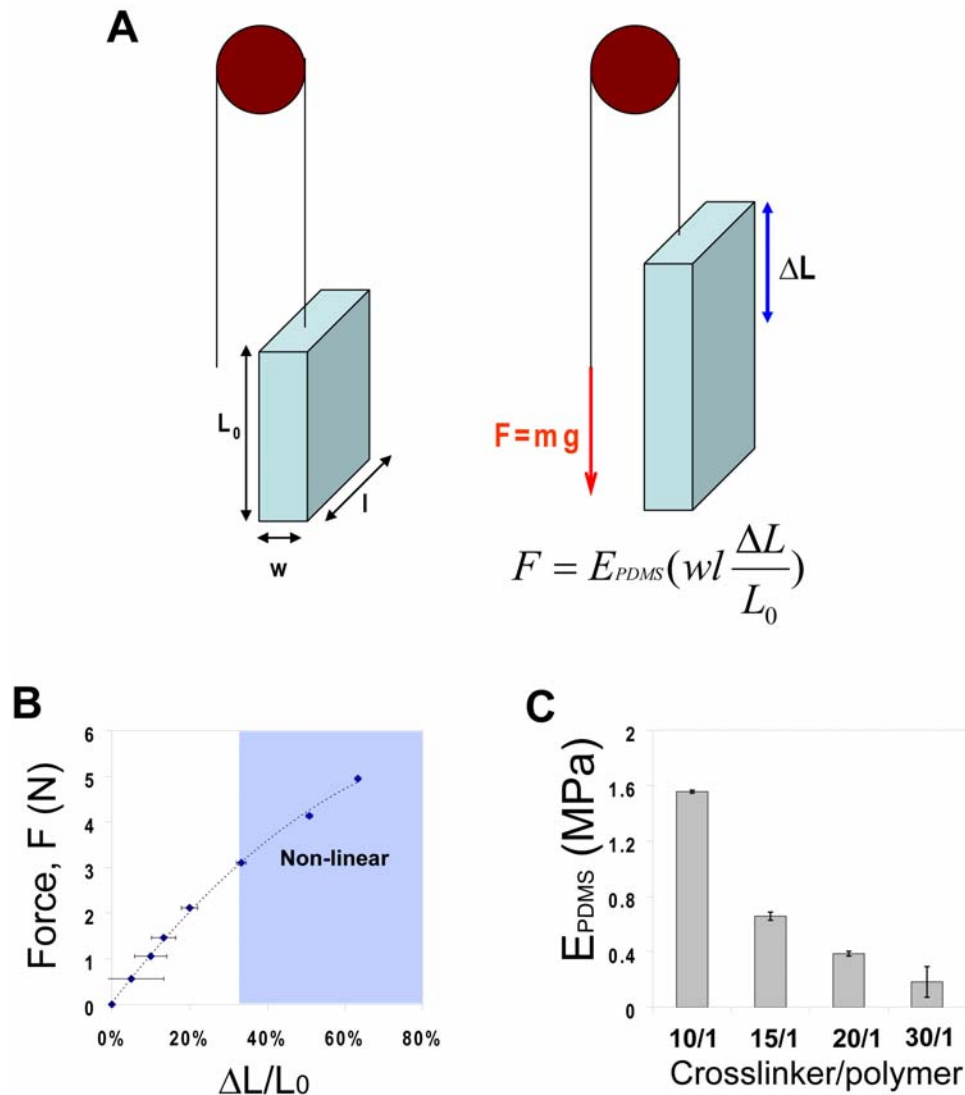


Figure S1

Figure S1. Tuning the Elasticity of PDMS Chambers

We varied the elasticity of PDMS by altering the ratio of crosslinker/polymer ratio. A) Schematic of a strain-stress experimental device used to measure the elasticity of the polymer: A large block of PDMS (typically 10cm* 4cm*1 cm) is attached to a fixed table at the bottom and to a rope at the top. The rope is connected to a basket through a pulley. Increasing weights are placed in the basket and the deformation is measured. B) Plot of the force as a function of the relative deformation of the PDMS block. Small deformations (up to 30%) are linear and allow for an estimate of the Young's modulus. For very large deformations, we can observe a saturation corresponding to a non-linear elastic response of the polymer. Error bars represent imprecision in the deformation measurements. C) Young's modulus of the PDMS as a function of the crosslinker/polymer ratio. Error bars represent standard deviations.

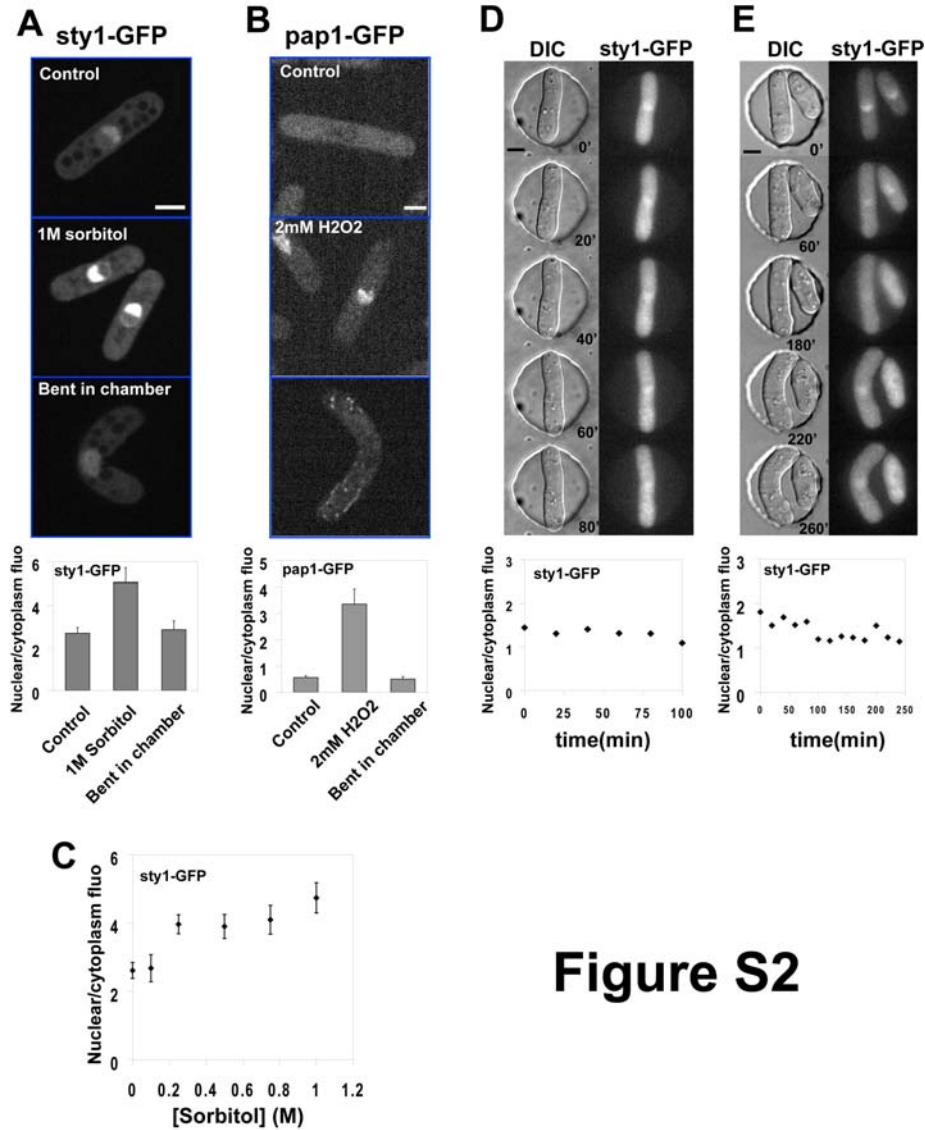


Figure S2

Figure S2. Bending and Growing Cells under Force Does Not Induce a Strong Stress Response

As markers of cellular stress, we imaged *sty1-GFP* and *GFP-pap1*. Both proteins are largely cytoplasmic in the absence of stress, and accumulate in the nucleus upon stress. A) Images of *sty1-GFP* cells (NM185) grown in normal media (control cells), immersed 5 min in 1 M sorbitol (osmotic stress) or bent in the chamber for 15 min in normal media. The graph shows quantification of the nuclear/cytoplasmic fluorescent ratios (n=10 cells/condition). B) Images of *GFP-pap1* cells (NM189) in normal media, treated for 5 min in 2mM H₂O₂ (oxidative stress), or bent in the chamber for 15 min in normal media. The graph shows quantification of the nuclear/cytoplasmic fluorescence ratios (n=10 cells/condition). C) Nuclear/cytoplasmic fluorescence ratios of *sty1-GFP* in cells immersed 5 min in media containing increasing concentrations of sorbitol (n=10 cells for each point). Error bars represent standard deviations. D) *Sty1-GFP* cells were imaged in time-lapse as they grow and deform a chamber. Graph shows the nuclear/cytoplasmic fluorescent ratio of *sty1-GFP* as a function of time. E) Time-lapse images of a cell growing and buckling itself in a chamber. Graph shows the nuclear/cytoplasmic fluorescent ratio as a function of time. Scale bar=5μm.

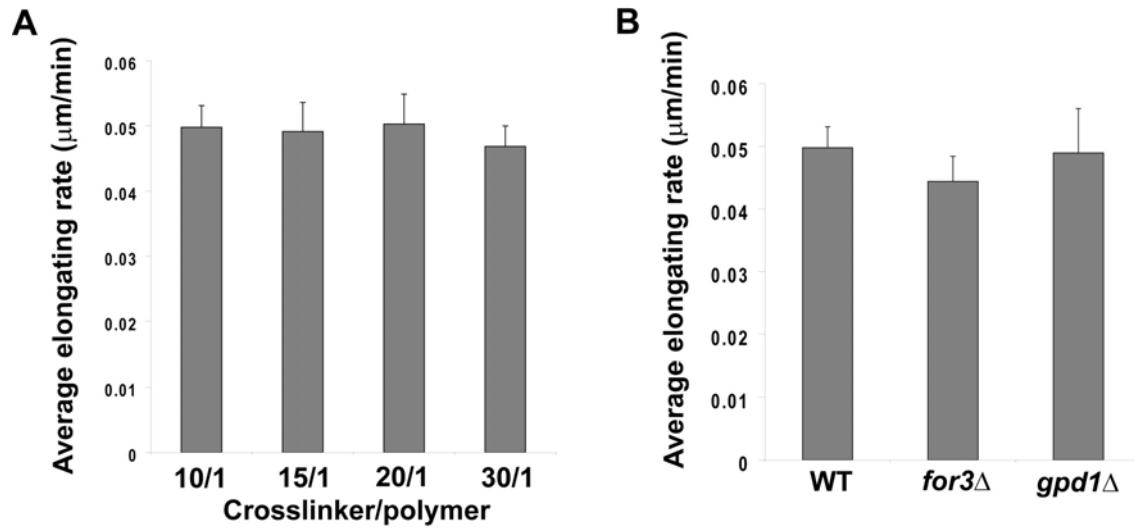


Figure S3

Figure S3 Growth Rates of Unconstrained Cells

A) Free average elongation rates of bipolar wild type cells in very large chambers of different elasticity (n=10 per condition). Error bars represent the standard deviation. The strain is NM11 (*cdc25-22* mutant, grown at 25°C). B.) Free average elongation rates of bipolar wild-type and mutant cells in very large chambers (n=10 per mutant). Error bars represent the standard deviation. The strains are NM11, NM209 and NM183 (all *cdc25-22* mutants, grown at 25°C).

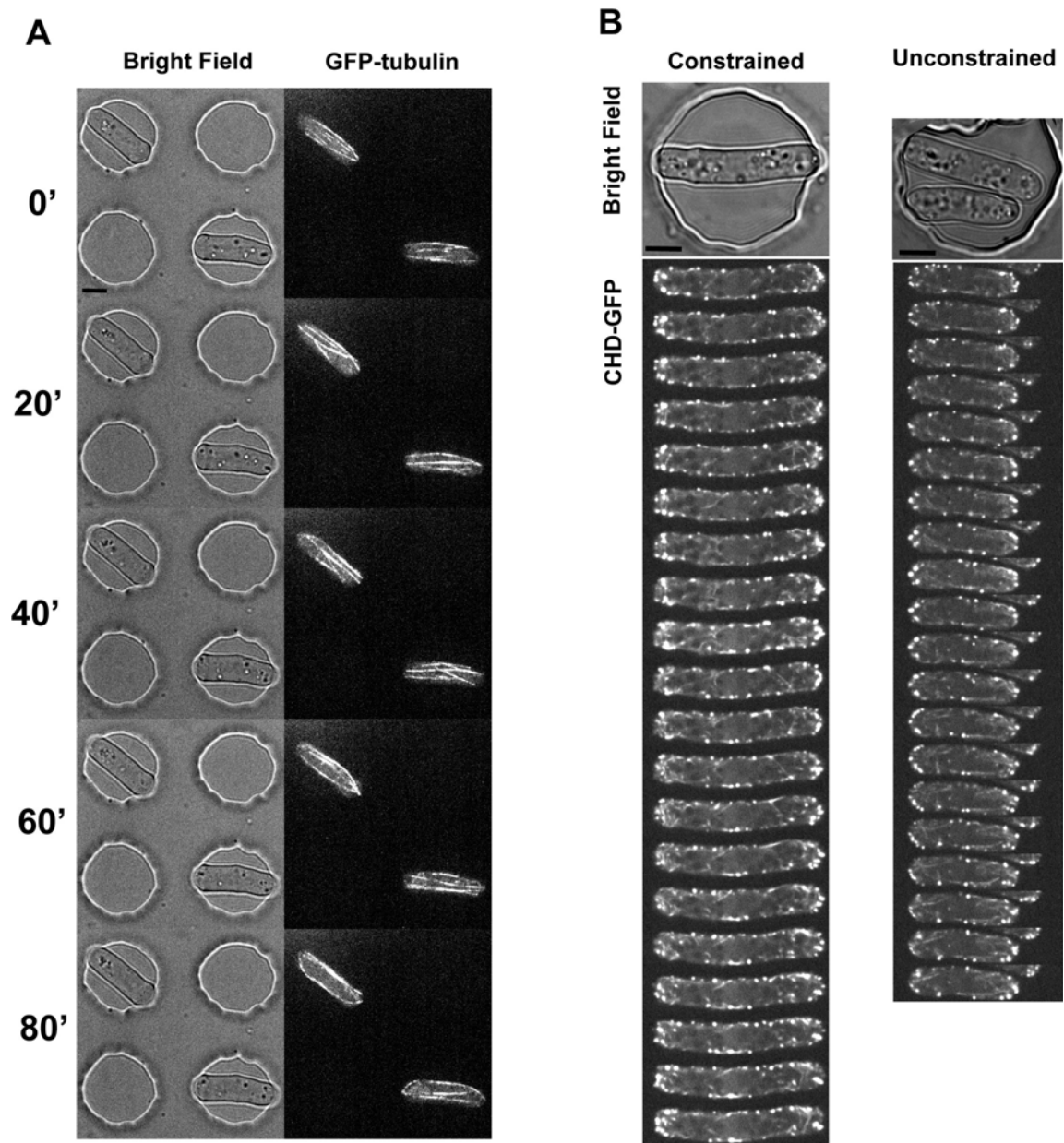


Figure S4

Figure S4 Microtubule and Actin Cytoskeletons Are Not Changed in Constrained Cells

A) Time-lapse images of cells expressing GFP-tubulin (NM11) while growing in and deforming soft chambers. Maximum intensity projection confocal images are shown. B) Time-lapse of cells expressing an actin marker CHD-GFP (Calponin homology domain) fusion protein (NM33), under constrained (left) and unconstrained conditions (right). 2s per slice. Scale bar=5 μ m.

Table S1. Strain List

FC1234		leu1-32:SV40:GFP-atb2[leu1+]
NM11	cdc25-22	leu1-32:SV40:GFP-atb2[leu1+]
NM33	cdc25-22	JK148-nmt41-GFP-CHD:leu1+
NM183	cdc25-22	gpd1::kanMX leu1-32:SV40:GFP-atb2[leu1+]
NM185	cdc25-22	sty1-GFP::kanMX
NM189	cdc25-22	leu1-32:nmt::GFP-pap1 [leu1+]
NM209	cdc25-22	for3::kanMX leu1-32:SV40:GFP-atb2[leu1+]